

Original

Kashaev, N.; Pugachev, D.; Riekehr, S.; Ventzke, V.:

**Fiber Laser Beam Welding of Ti-6242 - Effect of Processing
Parameters on Microstructural and Mechanical Properties**

In: Materials Science Forum, THERMEC 2016 (2016) Trans Tech Publications

DOI: [10.4028/www.scientific.net/MSF.879.903](https://doi.org/10.4028/www.scientific.net/MSF.879.903)

Fiber Laser Beam Welding of Ti-6242 – Effect of Processing Parameters on Microstructural and Mechanical Properties

Nikolai Kashaev^{1*}, Dmitry Pugachev¹, Stefan Riekehr¹
and Volker Ventzke¹

¹Helmholtz-Zentrum Geesthacht, Institute of Materials Research, Materials Mechanics,
Max-Planck-Str. 1, D-21502 Geesthacht, Germany

Keywords: laser beam welding, Ti-6242, butt joint, microstructure, tensile strength

Abstract. The present work investigates the effects of laser beam power, focus position and advance speed on the geometry, microstructure and mechanical properties of fiber laser beam welded Ti-6Al-2Sn-4Zr-2Mo (denoted as Ti-6242) butt joints used for high temperature applications. Detailed microstructural and mechanical studies were performed on welds produced using optimized parameters (a laser beam power of 5 kW, a focus position of 0.0 mm and an advance speed of 6.2 m/min). The Ti-6242 base material is characterized by a globular ($\alpha+\beta$) microstructure. The heat input during laser beam welding led to the formation of a martensitic α' -phase fusion zone. The heat affected zone consisted of globular grains and acicular crystallites. These local transformations were connected with a change in the micro-texture, average grain size and β -phase content. Furthermore, the microhardness increased from 330 HV 0.3 to 450 HV 0.3 due to the martensitic transformation. The mechanical behavior of the laser beam welded Ti-6242 butt joint loaded in tension was determined by the properties of the Ti-6242 base material. The local increase in hardness provided a shielding effect that protected the Ti-6242 butt joint against mechanical damage.

Introduction

The near- α α - β -titanium alloy Ti-6Al-2Sn-4Zr-2Mo (denoted as Ti-6242) was introduced in 1967 for high temperature applications in the high pressure compressor section of aero-engines, in which the temperature exceeds 350 °C and the more commonly used titanium alloy Ti-6Al-4V is unsuitable because of its poor creep performance [1,2]. Blades and discs are the typical applications for Ti-6242 [2]. Ti-6242 is also used in sheet-metal forming for engine afterburner structures and for various “hot” airframe skin applications [3].

Because thin sheet structures cannot be welded using diffusion bonding or friction welding and friction stir welding cannot be easily applied due to the high tool wear caused by the high strength of the titanium alloy, fusion welding processes (e. g. arc welding, electron beam welding and laser beam welding (LBW)) are required. Arc welding processes and electron beam processes for titanium alloys are well established [4,5]; however, there is little published data on LBW of Ti-6242 [6]. The current research aims to investigate the microstructure and mechanical performance of fiber laser beam welded Ti-6242 butt joints.

Laser beam welding and weld seam morphology

Commercially available Ti-6Al-2Sn-4Zr-2Mo sheets with a thickness of 2.0 mm were used for the LBW experiments. LBW of butt joints was performed using an 8.0 kW fiber laser (IPG YLS-8000) with fiber optics (300 μ m core diameter and 300 mm focal length) at a focus spot diameter of 600 μ m. Butt joints were welded autogenously in a 3-axis Ixion CNC machine. The welding direction was parallel to the transverse direction of the sheet specimens. Each specimen was held fixed in an open box, which was then filled with Ar shielding gas to protect the weld bead from ambient air during the LBW process. Prior to welding, the surface of the titanium sheets was cleaned by mechanical grinding. Metallurgical specimens were prepared using conventional procedures followed by a final vibration polish with an oxide polish suspension (OPS) compound.

Several specimens were etched and observed with optical light microscopy to determine the geometrical features of the welds. Visual inspection was also used to analyze the outer appearance of the weld seams with respect to the weld imperfections (e.g. undercuts and excess of penetration). X-ray inspection was used to determine the internal imperfections (e.g. porosity and cracks) of the welds.

Fig. 1(a) shows the effect of laser power, focus position and advance speed on the microstructure and geometry of the welds qualitatively. To evaluate the results, the specific heat input (in kJ/m), defined as the laser power (in kW) divided by the advance speed (in m/s), was introduced. As shown, full penetration of the weld can be achieved using a wide range of processing parameters, except when the specific heat input (22.5 kJ/m) was too low (Fig. 1(a), photo (i)). Welds similar to those obtained using conduction welding were achieved at specific heat inputs between 90 kJ/m and 240 kJ/m (low advance speeds combined with low laser powers, Fig. 1(a), photos (a), (d-1), (d-2) and (g)). As expected, increasing the focus position above the specimen surface increases the weld width (Fig. 1(a), photos (b-1) and (b-2); (d-1) and (d-2); (f-1) and (f-2); (h-1) and (h-2)). Cao et al. reported that with increasing specific heat input, the weld bead geometry evolves from an hourglass morphology to a wide, nearly rectangular shape using autogenous Nd:YAG LBW of Ti-6Al-4V, which can be achieved changing the welding mode from keyhole to conduction mode [7]. Welds produced using the highest possible laser power (8 kW) combined with the highest advance speed (8.0 m/min) are I-shaped (Fig. 1(a), photo (c)). Welds with an hourglass shape were obtained using other processing parameters. The use of an 8 kW fiber laser with laser optics that allows the generation of a laser beam with a large area of constant irradiance (top-hat profile) retains the narrow keyhole with a near constant diameter through the depth, which makes obtaining I-shape welds possible. However, the butt joints welded at the highest laser power combined with the highest advance speed show larger undercuts and underfills (Fig. 1(a), photo (c)), which were caused by evaporation of the welded material.

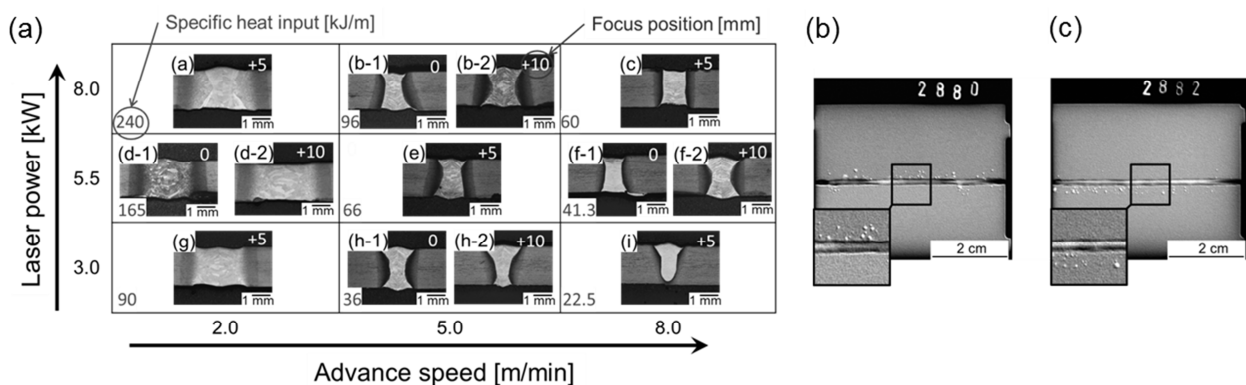


Fig. 1. (a) Effect of laser power, advance speed and focus position on geometry and microstructure of the butt-joints, and radiographs of (b) a weld with an irregular shape (focus position 0.0 mm, laser power 7 kW, advance speed 5.5 m/min) and (c) a weld with a more homogeneous shape (focus position 0.0 mm, laser power 5 kW, advance speed 6.2 m/min).

Using a focus position of 0.0 mm above the specimen surface, the second set of experiments with three laser power levels and four advance speeds was performed to identify the optimal processing parameters to produce butt joints with low porosity levels and regular shapes. The cross sections of the welds were investigated to determine the influence of the specific heat input on the geometry of welds. The dependence of the heat affected zone (HAZ) width and the fusion zone (FZ) width on the specific heat input are shown in Fig. 2. The widths of the HAZ and the FZ were measured in the cross-sections of the butt joints at three different positions: radiation exposure side, middle of the weld and rear side. A mean value of the HAZ width was calculated from the left and the right HAZ. The results indicate that the HAZ width increases with increasing specific heat input up to a specific heat input of 55 kJ/m and then remains relatively stable. The FZ width in the middle of the welds is relatively constant for the investigated specific heat inputs, but the values for the FZ width at the radiation exposure side and at the rear side of the joint showed more pronounced

fluctuations. The scatter of the FZ width values indicates that there are instabilities in the shape of the butt joints welded in this range of specific heat inputs.

The dependence of the HAZ/FZ width on the specific heat input for autogenous LBW of Ti-6Al-4V has been reported in the literature [8,9]. In the case of Ti-6242 a similar saturation effect from the formation of a conduction FZ surrounding the keyhole in the HAZ width vs. specific heat input behavior was observed (Fig. 2(a)). Fig. 2(a) and (b) clearly show that the formation of FZ and HAZ can be considered as inter-dependently. HAZ and FZ show simultaneous growth with increasing specific heat input up to approx. 55 kJ/m. After crossing this value the specific heat input is mainly consumed by the molten bath leading to a further gain of FZ while the HAZ width remains in the saturation condition. As long as there is sufficient heat dissipation into the BM, the HAZ width will be consistent. This explains the relatively constant values for the HAZ width in the specific heat input range from 55 kJ/m to 85 kJ/m. Because all of the butt joints showed low levels of defects, such as porosity, cracks and impurities, the identification of processing parameters for microstructural and mechanical investigations focused on the elimination of irregularities in the weld as shown in Fig. 1(b). Welds with a regular shape and without visible weld flaws were obtained using a laser beam power of 5 kW, a focus position of 0.0 mm and an advance speed of 6.2 m/min (radiograph in Fig. 1(c) and cross-section in Fig. 3(a)).

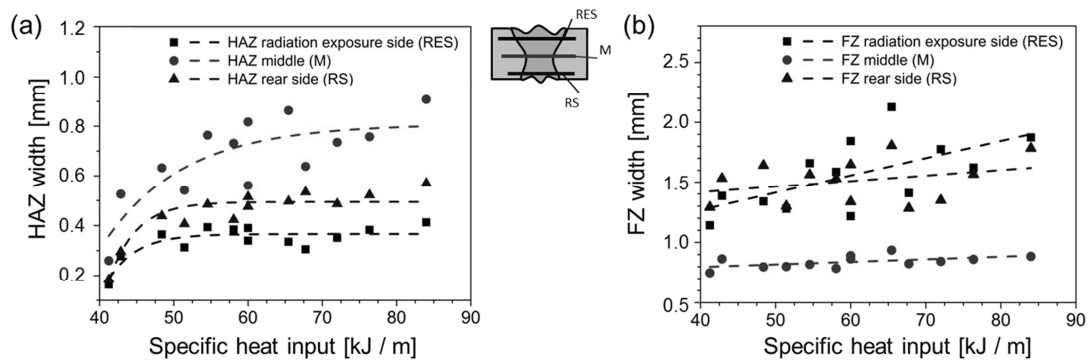


Fig. 2. (a) HAZ width and (b) FZ width vs. specific heat input for butt joints welded at a focus position of 0.0 mm above the specimen surface.

Microstructure

The microstructure of the laser beam welded Ti-6242 butt joint was investigated by scanning electron microscopy (SEM) (Jeol JSM-6490 LV) using electron back-scatter diffraction (EBSD) (EDAX TSL OIM) to determine local micro-texture, phase content and grain size within the BM, the HAZ and the FZ in order to analyze local changes activated by thermal cycling during the welding process. The EBSD measurements were performed at a voltage of 30 kV, an emission current of 75 μ A, a sample tilt angle of 70 $^{\circ}$, a working distance of 14 mm, a magnification of 750x and a step size of 0.5 μ m. The scan field size was 125 μ m x 125 μ m. The orientation calculation was based on the GSHE method, whereas triclinic sample symmetry was assumed. Microhardness profiles measured across the joint were obtained using an automated Vickers hardness testing machine with a 0.3 kg load. The metallographic samples used for EBSD analysis and microhardness testing were prepared by conventional multi-stage grinding and subsequent electrolytic polishing (60 % HClO₄ (60 ml) + (methanol + 2-butoxy-ethanol) (1000 ml)). Crystal orientations maps and recalculated inverse pole figures were used to determine the crystal orientations. The colors in the crystal orientation maps are based on the corresponding color coded inverse pole figure. The basal $\langle 0\ 0\ 0\ 1 \rangle$ crystal direction parallel to the surface normal direction (\parallel ND, [001]) is red, the prismatic $\langle 1\ 0\ -1\ 0 \rangle$ crystal direction is blue and the prismatic $\langle 2\ -1\ -1\ 0 \rangle$ crystal direction is green. Intermediate directions are characterized by corresponding intermediate colors.

The Ti-6242 BM consists of globular grains with an average grain size of 3.4 μ m \pm 1.2 μ m (Fig. 3(b)). Phase analysis indicates that the BM contains 7.5 % β -phase. The equiaxed grains are due to recrystallization that resulted from deformation and subsequent solution annealing in the (α + β)-

phase field [10]. Blue is the predominant color in the crystal orientation map of the BM (Fig. 3(b)). This means that a large number of grains are oriented in the $\langle 1\ 0\ -1\ 0 \rangle // \text{ND}$ direction, which is confirmed by the recalculated inverse pole figure showing a maximum axis intensity of $H = 5.7$ mrd at the $\langle 1\ 0\ -1\ 0 \rangle // \text{ND}$ corner). Furthermore, the intensity distribution spreads into the $\langle 0\ 0\ 0\ 1 \rangle // \text{ND}$ and the $\langle 2\ -1\ -1\ 0 \rangle // \text{ND}$ crystal directions. This regular spreading explains the appearance of purple, green and red coded grains in the crystal orientation map. The preferential orientations around the $\langle 1\ 0\ -1\ 0 \rangle // \text{ND}$ direction are the result of the rolling involved in the Ti-6242 processing.

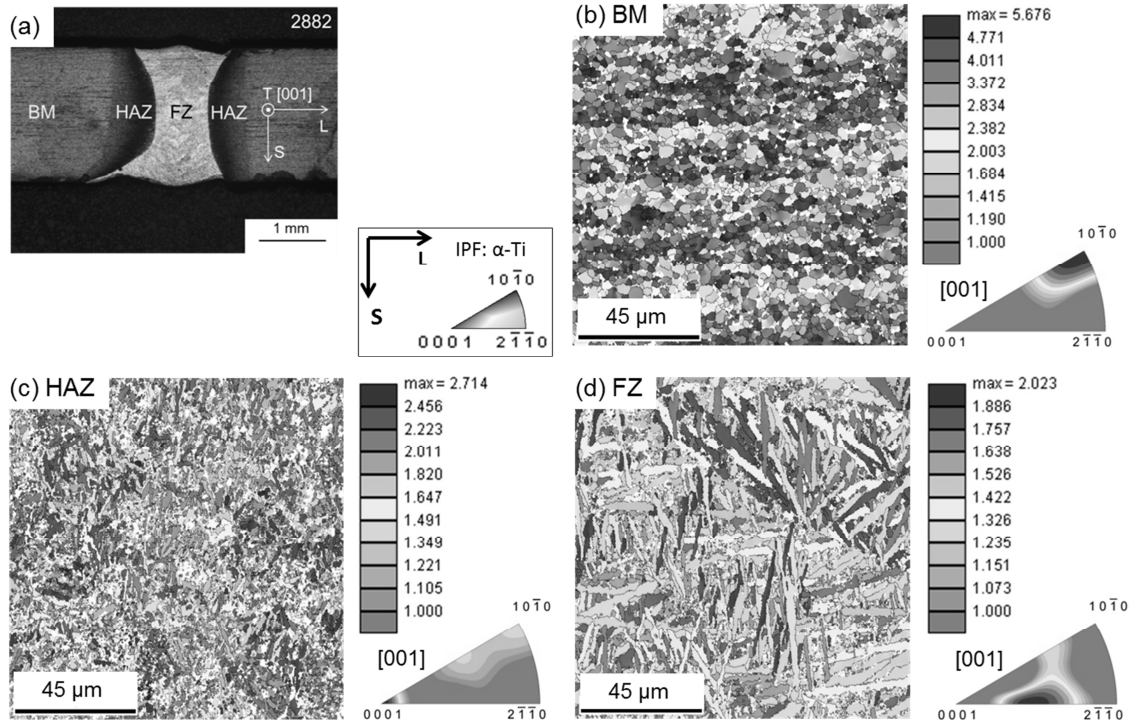


Fig. 3. (a) Cross section of the butt joint (L, S and T denote the longitudinal, thickness and transverse directions, respectively), and crystal orientation maps with inverse pole figures of (b) the equiaxed Ti-6242 BM ($L = 16$, $H_{\max} = 5.7$ mrd, $d = 3.4\ \mu\text{m} \pm 1.2\ \mu\text{m}$, β -phase content: 7.5 %), (c) the Ti-6242 HAZ ($L = 13$, $H_{\max} = 2.7$ mrd, $d = 2.1\ \mu\text{m} \pm 0.7\ \mu\text{m}$, β -phase content: 11.9 %) and (d) the Ti-6242 FZ ($L = 13$, $H_{\max} = 2.0$ mrd, $d = 4.9\ \mu\text{m} \pm 1.3\ \mu\text{m}$, β -phase content: 3.7 %).

A significant morphological change is observed within the HAZ adjacent to the FZ. The thermal cycling during the LBW of the Ti-6242 and the subsequent cooling resulted in a transformation of the equiaxed grains into acicular grains and embedded globular grains (Fig. 3(c)). The HAZ formation was associated with a grain refinement to an average grain size of $2.1\ \mu\text{m} \pm 0.7\ \mu\text{m}$ and an increase in the β -phase content to 11.9 %. The present HAZ microstructure can be considered as a mixture of a martensitic α' -phase and primary α - and β -phases. The increase in the β -phase content is due to processing temperatures higher than the beta transus of Ti-6242 ($993\ \text{C}^\circ - 995\ \text{C}^\circ$ [3]). Orhan et al. [11], Islam et al. [12] and Salehi et al. [13] reported that the volume fraction of the β -phase increased with temperature in a Ti-6Al-4V alloy. It is assumed that the HAZ of laser beam welded Ti-6242 shows a similar reaction because the formation of acicular crystals requires both temperatures higher than the beta transus and subsequent rapid cooling from the β -phase field to the $(\alpha+\beta)$ phase. The recalculated inverse pole figure shows that grains oriented in the $\langle 0\ 0\ 0\ 1 \rangle // \text{ND}$ crystal direction with spread angles of approximately 20° were found in the HAZ, whereas the axis intensity of the $\langle 1\ 0\ -1\ 0 \rangle // \text{ND}$ crystal direction is lower compared to the BM. The comparison shows a tilting of the $\langle 0\ 0\ 0\ 1 \rangle // \text{ND}$ crystal direction at an angle of approximately 90° occurred during the microstructure transformation. The center of the FZ (Fig. 3(d)) reveals a martensitic microstructure with an average grain size of $4.9\ \mu\text{m} \pm 1.3\ \mu\text{m}$ and a β -phase content of 3.7 %. The present microstructure was formed by cooling along the reaction path $\beta \rightarrow (\alpha+\beta)$, whereas a diffusionless transformation from the β -phase to the martensitic α' -phase led to the formation of a

needlelike microstructure in the FZ. The crystal orientation map indicates that, unlike in the HAZ and the BM, preferred orientations are not present in the FZ. The recalculated inverse pole figure shows two maxima: at $\langle 8 \ -4 \ -4 \ 9 \rangle // \text{ND}$ ($H = 2.0$ mrd) between $\langle 8 \ -4 \ -4 \ 29 \rangle // \text{ND}$ and $\langle 4 \ -2 \ -2 \ 1 \rangle // \text{ND}$ and at $\langle 3 \ 0 \ -3 \ 2 \rangle // \text{ND}$ ($H = 1.3$ mrd) between $\langle 0 \ 6 \ -6 \ 7 \rangle // \text{ND}$ and $\langle 0 \ 5 \ -5 \ 2 \rangle // \text{ND}$. This distribution explains the appearance of intermediate colors in the crystal orientation map and suggests that the fraction of pyramidal crystal planes in the FZ is higher than in either the BM or the HAZ. The cooling rate within the HAZ adjacent to FZ was sufficiently high to partially activate the diffusionless $\beta \rightarrow \alpha'$ transformation, which resulted in the formation of acicular crystals. Metallographic examinations reveal that the HAZ adjacent to the BM consisted of globular grains.

Mechanical properties

Microhardness was measured across the weld in three regions of the cross-section: radiation exposure side, middle side and rear side, as shown in Fig. 4(a). The three measured microhardness profiles are similar. The indentation within the BM was parallel primarily to $\langle 1 \ 0 \ -1 \ 0 \rangle // \text{ND}$ crystal direction. The continuous increase of hardness within the HAZ from the BM to the FZ is due to the increasing amount of martensitic α' -phase. The martensitic α' -phase provides high strength and hardness accompanied by a loss of ductility and toughness. The effect of the accumulation of grains oriented in the $\langle 0 \ 0 \ 0 \ 1 \rangle // \text{ND}$ crystal direction in the HAZ adjacent to the FZ cannot be neglected.

Standard tensile tests were performed at ambient temperature according to the DIN EN ISO 6892-1:2009. The load-bearing cross section of the tensile specimen was $12.5 \text{ mm} \times 2.0 \text{ mm}$, with a total specimen length of 165 mm. A 100 kN electro-mechanical universal testing machine with a constant transverse main displacement was used. The elongation of the specimen was measured with a laser extensometer with an initial length, l_0 of 50 mm. For the welded specimen, the weld was always located exactly in the center of l_0 . The results of the tensile tests are represented in Fig. 4(b). As expected from the microstructure, the tensile behavior of the Ti-6242 sheet depends on the test direction because of the anisotropy of the hcp α -phase. The laser beam welded Ti-6242 butt joint fractured within the BM. The condition of the HAZs and the laser beam weld did not influence the mechanical behavior of the butt joint under a static tensile load because they had yield strengths higher than the BM.

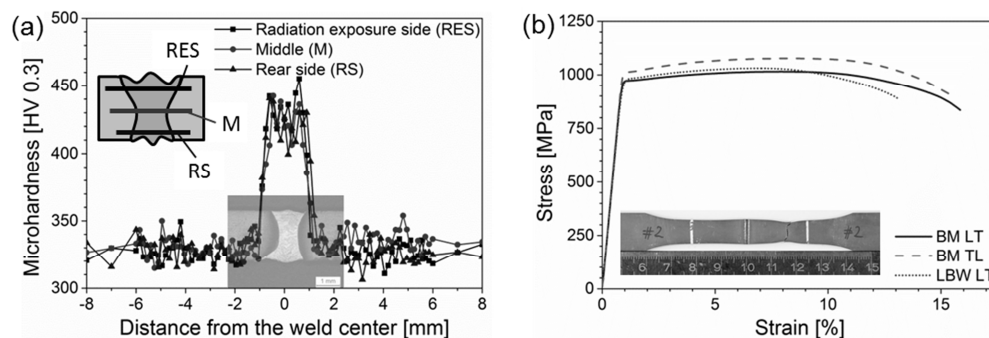


Fig. 4. (a) Microhardness and (b) tensile test results. “LT” – loading in longitudinal direction of the sheet, “TL” – loading in transverse direction of the sheet.

Summary

A LBW process for Ti-6242 was developed to optimize the microstructure and mechanical properties. The following conclusions can be drawn:

- (1) Autogenous LBW of Ti-6242 butt joints was investigated with regard to morphological and geometrical characteristics of the weld. Welds with a low porosity level and appropriate seam geometry were obtained.
- (2) The laser beam welded Ti-6242 butt joint exhibited a martensitic FZ, an inhomogeneous HAZ and a recrystallized BM. The HAZ adjacent to the BM consisted of globular grains. This

microstructure changed to a mixture of α -phase, martensitic α' -phase and β -phase. The thermal cycling changed the average grain size, β -phase content and micro-texture of the welds.

(3) The microhardness profiles showed a continuous increase within the HAZ from the BM to the FZ because of the increasing amount of martensitic α' -phase.

(4) The mechanical behavior of the laser beam welded Ti-6242 butt joints in tension was determined by the properties of the Ti-6242 BM despite the presence of geometrical notches in the samples. The local increases in hardness provide a shielding effect and protect the Ti-6242 butt joint from mechanical damage.

References

- [1] Properties of nonferrous heat-resistant materials, in: J. R. Davis (ed.), Heat-resistant Materials, ASM International, Materials Park, USA, 1997, pp. 345-438.
- [2] High temperature alloys, in G. Lütjering, J.C. Williams (Eds.), Titanium, Springer, Berlin, Heidelberg, 2003, pp. 259-279.
- [3] R. Boyer, G. Welsch, E.W. Collings (Eds.), Materials Properties Handbook: Titanium alloys, ASM International, Materials Park, USA, 1994.
- [4] F.D. Mullins, D.W. Becker, Weldability Study of Advanced High Temperature Titanium Alloys, Weld. Res. Suppl. 59 (1980) 177s-182s.
- [5] R. Pederson, F. Niklasson, F. Skystedt, R. Warren, Microstructure and mechanical properties of friction- and electron-beam welded Ti-6Al-4V and Ti-6Al-2Sn-4Zr-6Mo, Mater. Sci. Eng. A-Struct. 552 (2012) 555-565.
- [6] F. Torster, J.F. dos Santos, M. Kocak, M. Penasa, Mechanical and microstructural characterization of laser beam welded titanium alloys, in: Proc. 5th International Conference on Trends in Welding Research, ASM International, Materials Park, Ohio, USA, 1999, pp. 887-892.
- [7] X. Cao, A.S.H. Kabir, P. Wanjara, J. Gholipour, A. Birur, J. Cuddy and M. Medraj, Global and local mechanical properties of autogenously laser welded Ti-6Al-4V, Metall. Mater. Trans. A 45A (2014) 1258-1272.
- [8] A. Squillace, U. Prisco, S. Ciliberto, A. Astarita, Effect of welding parameters on morphology and mechanical properties of Ti-6Al-4V laser beam welded butt joints, J. Mater. Process. Technol. 212 (2012) 427-436.
- [9] X. Cao, M. Jahazi, Effect of welding speed on butt joint quality of Ti-6Al-4V alloy welded using a high-power Nd:YAG laser, Opt. Lasers Eng. 47 (2009) 1231-1241.
- [10] J.R. Wood, P.A. Russo, M.F. Welter, E.M. Christ, Thermomechanical processing and heat treatment of Ti-6Al-2Sn-2Zr-2Cr-2Mo-Si for structural application, Mater. Sci. Eng. A-Struct. 243 (1998) 109-118.
- [11] N. Orhan, T.I. Khan, M. Eroglu, Diffusion bonding of a microduplex stainless steel to Ti-6Al-4V, Scripta Mater. 45 (2001) 441-446.
- [12] M.F. Islam, J. Pillin, N. Ridley, Effect of surface finish and sheet thickness on isostatic diffusion bonding of superplastic Ti-6Al-4V, Mater. Sci. Tech. 13(12) (1997) 1045-1050.
- [13] M.T. Salehi, J. Pilling, N. Ridley, D.L. Hamilton, Isostatic diffusion bonding of superplastic Ti-6Al-4V, Mater. Sci. Eng. A-Struct. 150 (1992) 1-6.